Expanding the toolbox for nanoparticle trapping and spectroscopy with holographic optical tweezers

Expanding the toolbox for nanoparticle trapping and spectroscopy with holographic optical tweezers

M Dienerowitz[1], G Gibson[1], F Dienerowitz[2] and M Padgett[1]

[1] SUPA, School of Physics and Astronomy, University of Glasgow, Glasgow G12 8QQ, UK
[2] Institute of Engineering Mechanics (Institut für Technische Mechanik, ITM), Karlsruhe Institute of Technology (KIT), 76131 Karlsruhe, Germany

E-mail: maria.dienerowitz@glasgow.ac.uk

Abstract
We have developed a workstation based on holographic tweezers to optically trap, move and characterize metal nanoparticles. Our advanced darkfield imaging system allows us to simultaneously image and take spectra of single trapped metal nanoparticles. We take advantage of the beamshaping abilities of the spatial light modulator and correct for aberrations of the trapping optics. We monitor the improvement of the optical trap with video-based nanoparticle tracking. Furthermore we theoretically assess the capabilities and limitations of video-based tracking for nanoparticle position detection, in particular with respect to acquisition frequencies below the corner frequency.

Keywords: holographic optical tweezers, nanoparticle trapping and spectroscopy, darkfield imaging, video-based particle tracking

S Online supplementary data available from stacks.iop.org/JOpt/14/045003/mmedia

(Some figures may appear in colour only in the online journal)

1. Introduction

Optical trapping of metal nanoparticles [1–3] offers new applications for nano- and biotechnology including non-invasive probes for sensing and imaging [4, 5]. Optical tweezers provide three-dimensional position control of nanoparticles and allow the study of their electromagnetic interactions and spectral properties away from interfering interfaces [6]. Over recent years a number of experiments have increased the variety of nanoparticles trapped with single beam tweezers [7, 8]. A specific feature of metal nanoparticles is their plasmon resonance, which can lead to strong local field enhancements and heating. To avoid the latter a trapping laser far from the resonance frequency and a well-optimized trapping beam are essential [9]. It has also been shown that local field enhancements support nonlinear effects at the trap site exhibiting a range of new phenomena [10].

The nanoparticle workstation combines holographic tweezers with both darkfield imaging and spectroscopy. It enables us to create multiple aberration corrected optical traps and simultaneously image and track the positions of the nanoparticles as well as taking their individual spectra. The holographic tweezers system is based on a spatial light modulator (SLM). The SLM splits the laser into several optical traps with both individual settings for position and global beam corrections such as astigmatism [11]. We are able to manipulate trapped configurations of metal nanoparticles across the entire field of view (50 μm) as shown in figure 1 (and multimedia available at stacks.iop.org/JOpt/14/045003/mmedia). Standard darkfield imaging is based on a viewing objective with a restricted numerical aperture, which is unsuitable for 3D optical trapping. We developed a darkfield imaging system without restricting the high numerical aperture of our trapping objective by accessing
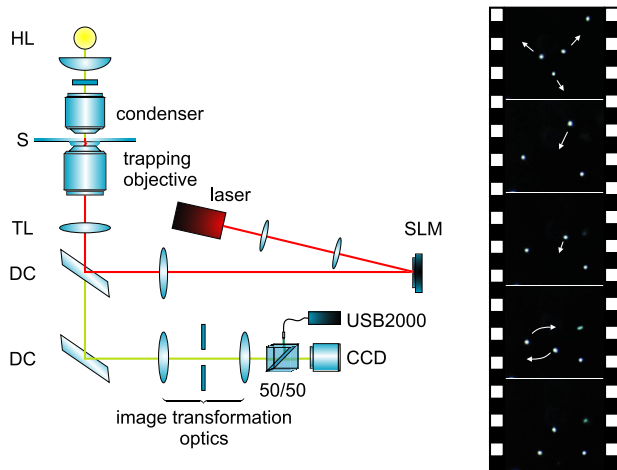
2. Holographic tweezers setup

The holographic workstation is based around a purpose-built inverted microscope with the addition of a Ti:sapphire laser (M squared, SolsTiS, 1.5 W, 790–850 nm). A standard Zeiss illumination carrier holds a tungsten halogen light source and a darkfield condenser (Zeiss, 0.9 NA) to illuminate the sample. An additional telescope in the imaging train is the central part of our darkfield imaging system, which we discuss in section 3. Figure 1 shows the optical path of the trapping laser, which we expand to fill the active region of the SLM (Boulder Nonlinear Systems, XY Series, 512 pixels × 512 pixels). The laser then passes another telescope which images the SLM to the back aperture of the microscope objective (Nikon, CFI Plan Fluor, oil immersion with iris NA 0.5–1.3) before entering the sample cell. The sample cell confines a drop of diluted 100 nm gold (BBInternational) nanoparticle solution between two coverslips. An *x–y–z* stage (ASI MS-2000 with integrated ASI LS-50-M) holds the sample cell and moves the microscope objective axially for focusing. We implemented the control of all devices into LabVIEW software (National Instruments) [22] along with particle tracking, image and spectra acquisition.

3. Imaging and spectroscopy

Darkfield imaging provides a high contrast image of metal nanoparticles in solution. It is the ideal technique to image and track optically trapped nanoparticles as well as directly accessing their scattering spectra. So far the constraining factor has been the complementary conditions for the condenser and trapping objective lens. For darkfield illumination the numerical aperture (NA) of the condenser lens has to be larger than the NA of the viewing objective. The condenser contains a darkfield stop such that without a sample no light reaches the imaging sensor. This restriction on the numerical aperture on the objective lens is incompatible with optical trapping, which needs to have an NA as large as possible. We resolve this issue by inserting an additional telescope after the first image plane behind the tube lens. In this way we are able to access the Fourier plane of our sample and filter out the unwanted components of the illumination in the imaging path beyond the trapping laser path. Figure 2 gives a detailed overview of the imaging optics as well as sample images obtained with two variants of our darkfield imaging method.

We have two options to acquire darkfield images of our sample, depending on the condenser we choose to use. For a standard darkfield condenser we block the collected ring of illumination with an adjustable iris in the Fourier plane of the sample and obtain a high contrast darkfield image of the trapped nanoparticles. It is also possible to use standard brightfield illumination and subsequently insert a correctly sized centre stop in the Fourier plane. The centre stop blocks the on-axis brightfield illumination while allowing light scattered at large angles to pass. The information content of the scattered light is contained beyond the centre region and therefore still able to reach our camera or spectrometer.

Figure 1. The diagram shows the layout of the nanoparticle workstation with the laser (red) and imaging (green) beam paths including halogen illumination HL, sample S, tube lens TL, dichroic DC, Ocean Optics USB2000 spectrometer and the spatial light modulator (SLM) in the Fourier plane of the sample. We placed the image transformation optics outside the laser beam path to not affect the trapping performance of our workstation (see multimedia file available at stacks.iop.org/JOpt/14/045003/mmedia).

the sample's Fourier plane outside the laser beam path. Our improved darkfield system provides excellent images and also direct access to the nanoparticles' scattering spectra.

Trapping of metal nanoparticles is challenging because of their subwavelength dimensions and large scattering cross section. Consequently, trapping in 3D requires low beam aberrations to minimize the required laser power and avoid the nanoparticles being pushed out of the focus by the scattering force. Tracking the variance of the trapped particle's position gives a measure of the quality of the trap. Video-based particle tracking is very easy to implement and capable of tracking several particles simultaneously [12]. However, it has not been used to track metal nanoparticles as it is challenging to obtain a quality image at high acquisition speed. The latter is important, as metal nanoparticles tend to have corner frequencies of several hundred Hz, requiring acquisition frequencies of several kHz at low light levels. Quadrant photodiode tracking does provide this speed [7, 8, 13]; however, combining it with darkfield imaging and multiple traps appears cumbersome [14].

Recent advances in video-based tracking have demonstrated acquisition frequencies of several kHz for tracking micron-sized beads [15, 16]. However the challenge remains to generate a bright, high-quality image of a nanoparticle. Although darkfield imaging of metal nanoparticles is well established, the combination of darkfield imaging and optical trapping has only been realized over the past year [17–19]. By taking into account the limitations of motion blur and undersampling [20, 21] we video-track metal nanoparticles to monitor the improvement of trap performance after aberration correction. We analyse the variance of the particle's position distribution with respect to acquisition frequency and compare these results with our experimental data.
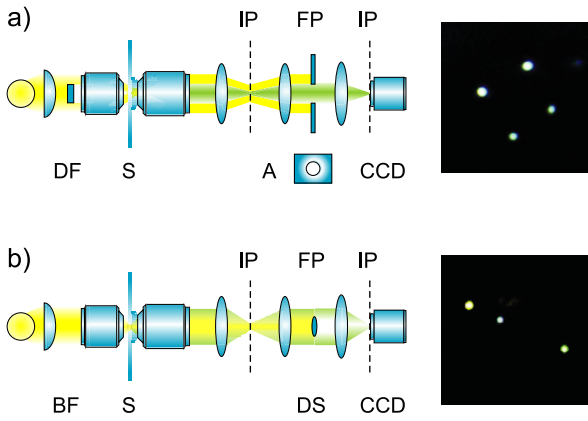
Figure 2. (a) We relay the image plane IP with an additional telescope to access the Fourier plane FP of our sample. By inserting an iris A into the FP we are able to block the ring-shaped darkfield illumination DF collected with the high NA trapping objective. (b) In the same way as described for (a) we use standard brightfield illumination BF to obtain a darkfield image by inserting a centre stop DS into the FP of the sample.

Both imaging methods give darkfield images by eliminating the background illumination and image the scattered light of the nanoparticles, which we record with a high-speed camera (Prosilica GE680C). By inserting a 50/50 visible beam splitter we are able to take spectra of single particles while monitoring their position with the camera. We use an Ocean Optics USB2000 spectrometer to measure the spectrum from a specific location within our field of view. In this way we are able to associate a single spectrum to an individual particle and monitor the spectrum's change upon particle interactions. The spectrum of a metal nanoparticle displays a characteristic peak at the wavelength of the plasmon resonance. The wavelength as well as the width of

the peak depend on the size, material and shape of the particle and enable us to distinguish single particles from dimers or clusters. The plasmon resonances of two individual particles interact if their separation distance is of the same order as their diameters [1, 23]. Note that the plasmon resonance is excited by the tungsten halogen illumination, not the trapping laser.

To investigate the resonant coupling of trapped particles further, we changed the distance between two nanoparticles by moving individual traps. The particles undergo Brownian motion with an amplitude of approximately 400 nm within the trap. By overlapping the two traps or loading both particles into the same trap we were able to observe plasmonic coupling between the two particles. Upon dimerization of two nanoparticles, the plasmon resonance broadens and red-shifts. If the nanoparticles only reside within the same trap without interaction we observe a spectrum, which is the sum of the individual spectra of the particles. The moment the nanoparticles come into close contact, the maximum of the recorded spectrum clearly shifts towards longer wavelengths and broadens compared to the sum of the individual spectra, as expected [1].

We present our results in figure 3, comparing the coupling and non-coupling cases. In our experiment the number of coupling events was much smaller than the non-coupling ones (approximately 5%). Even improvement of the trap, which leads to a tighter confinement of the trapped particle (see section 4), did not result in an increase in coupling events. We conclude that the optical forces exerted by the trapping laser are not the dominant forces in this process. The electrostatic forces determined by the individual surface charges of the nanoparticles play a more important role, and in many cases prevent coupling. We would anticipate an increase in coupling events by adjusting the salt concentration of the sample solution [23]. Furthermore, the interacting resonances result in additional forces, which need to be taken into account [24].

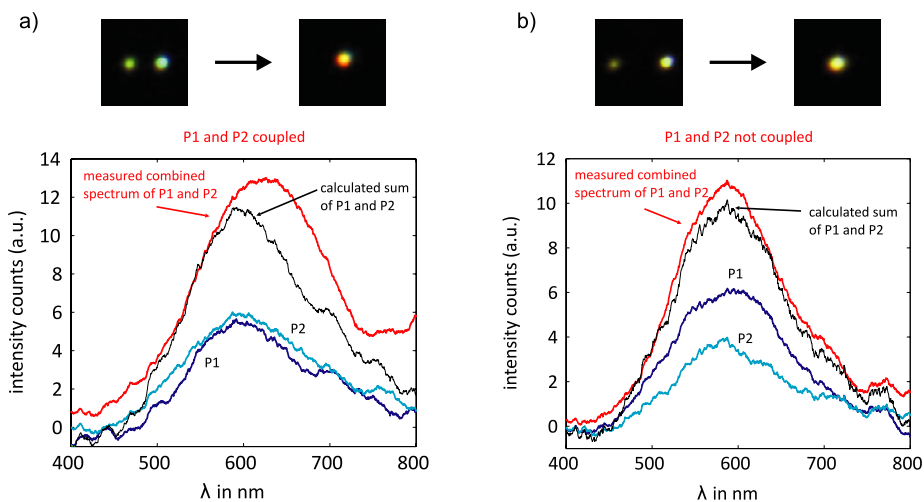**Figure 3.** Initially, we take the spectra for individually trapped nanoparticles denoted by P1 and P2. Then we place both particles in the same trap and take the combined spectrum of both particles. Comparing this spectrum with the calculated sum of P1 and P2 indicates whether the plasmon resonances of the individual particles interact (a) or the nanoparticles simply reside next to each other without interacting (b).
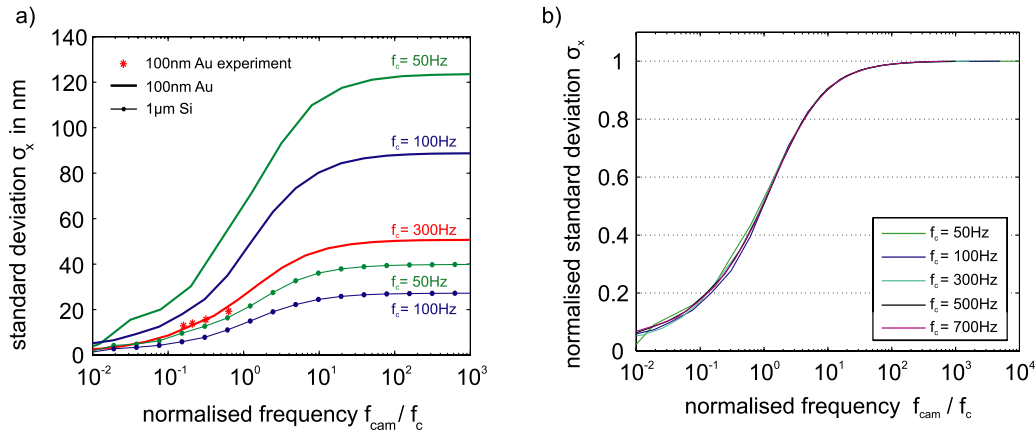
Figure 4. (a) We simulated the Brownian motion of a trapped 100 nm gold sphere and a 1 μm silica sphere as described in more detail in the text. We then determined the standard deviation σ_x of the particle's position distribution depending on the camera acquisition frequency f_{cam} normalized with the corner frequency f_c. The standard deviation of a micron-sized silica sphere is a lot smaller compared to σ_x of a 100 nm gold sphere, which explains why the former are so much easier to trap. Our results show that the f_{cam} should be 10–20 times higher than f_c to avoid motion blur. (b) This relationship becomes even clearer when viewing the same data with normalized standard deviation $\sigma_x / \max(\sigma_x)$.

4. Particle tracking and aberration correction

One advantage of holographic tweezers is the ability to control the beam shape of the trapping laser and correct for aberrations [25, 26]. This is an important factor, as trapping of metal nanoparticles requires the best possible beam focusing. To assess the improvement achieved by beam shaping we monitor the standard deviation $\sigma_x = \sqrt{\text{var}(x)}$ of the trapped nanoparticle's position distribution. The standard deviation σ_x is directly linked to the optical trap stiffness κ_x by $\sigma_x^2 = \text{var}(x) = k_B T / \kappa_x$ and corner frequency f_c by $\sigma_x^2 = k_B T / (2\pi \gamma f_c)$ with the drag coefficient $\gamma = 6\pi \eta R$. It is almost impossible to obtain high-quality brightfield images of nanoparticles for particles smaller than 100 nm as they are below the diffraction limit. Darkfield imaging renders even much smaller particles visible, however at the price of lower light levels of the image. By choosing a video-based tracking system for nanoparticles in darkfield illumination, we are limited in the acquisition speed by the lack of light compared to imaging micron-sized beads in brightfield illumination.

Our camera is capable of sampling at 1 or 2 kHz when restricting the field of view to a small region of interest (5 μm). However this is only useful for bright images with the exposure time set to a minimum. With our present darkfield illumination we have to increase the camera's exposure time, which limits our acquisition frequency to 200 Hz. The reduced acquisition frequency introduces motion blur to the acquired images of the trapped particles by time-averaging the particles' positions over the integration time. This reduces the standard deviation of the particles' position distribution and hence suggests a much stiffer trap than actually present [20, 21].

A common concern with video tracking is the risk of undersampling the position data. This is a problem when analysing the power spectrum of the trapped particle's position in frequency space or reconstructing the particle's trajectory. Trapped metal nanoparticles have large trap stiffnesses and corner frequencies up to several hundred Hz. Our acquisition frequency is below the corner frequency of the trapped nanoparticle and we will therefore undersample the position distribution. However, undersampling does not affect the standard deviation of the position distribution if the particle's motion is monitored for a sufficient length of time. On the contrary, motion blur significantly distorts the position data and has to be taken into account. The question remains by how much we underestimate the standard deviation due to motion blur. And also, is it possible to use video tracked positions to compare the trap stiffnesses for different beam correction settings and conclude on an optimal trap? In order to answer this question we simulated the motion of a trapped nanoparticle subjected to Brownian motion according to the Langevin equation

$$m\ddot{x} + \gamma \dot{x} + \kappa x = \sqrt{2k_B T \gamma}\, \eta(t). \tag{1}$$

Here we neglect the first term, as the motion of the particle is highly overdamped. Replacing the trap stiffness $\kappa = 2\pi \gamma f_c$ we obtain the well-known equation of motion of an overdamped optically trapped particle in a harmonic potential subjected to Brownian motion [13]:

$$\dot{x} + 2\pi f_c x = \sqrt{2k_B T / \gamma}\, \eta(t). \tag{2}$$

We compare simulation data of a 100 nm gold sphere and a 1 μm silica bead for different corner frequencies f_c in figure 4. For each data point we average over 40 simulations, each calculating the position of the trapped particle with a step size of 1 μs for a total time of 4 s. We then successively increase the integration time sampling the simulated data to find a relationship between the standard deviation σ_x of the position distribution and the camera acquisition frequency f_{cam}. To simulate a decrease in camera acquisition frequency f_{cam} we increase the integration time sampling the simulated data. This averages the position of the trapped particle subjected to Brownian motion just as a longer integration time of the camera in the experiment would do.
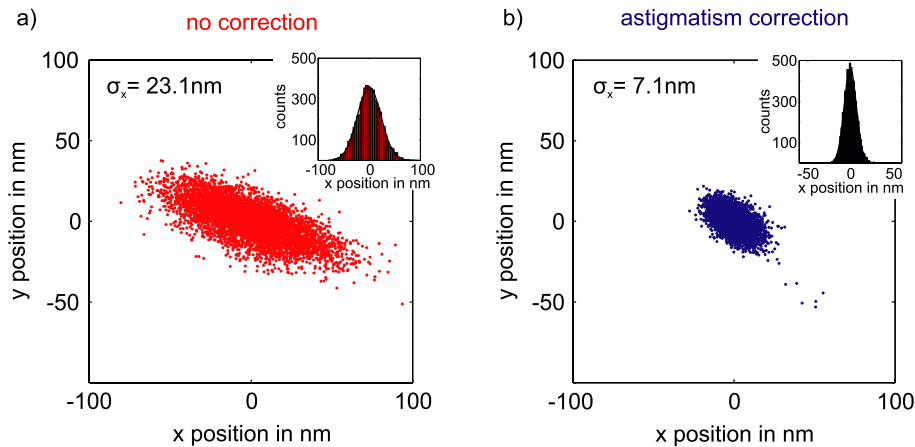
a) no correction   b) astigmatism correction

Figure 5. We plot the position distributions and histograms for a trapped 100 nm gold sphere before (a) and after (b) correcting for astigmatism of the trapping beam. We are able to improve the spatial confinement of the nanoparticle in the trap by a factor of 3. The ratio of σ_x^{before} and σ_x^{after} gives an absolute measure of trap improvement even though we underestimate σ_x due to our small sampling frequency f_{cam}.

Our simulations confirm that the decrease of the standard deviation due to motion blur is predictable [20, 21]. The differences in σ_x between the gold nanoparticles and the silica beads show why it is hard to trap nanoparticles: for the same corner frequency their position distribution is much wider than for a micron-sized bead. By normalizing the acquisition frequency f_{cam} with the corner frequency f_c the universal relationship between σ_x and f_{cam} is revealed and confirmed in figure 4(b). All different corner frequencies are now described by a general relationship between the acquisition frequency and the amount of undersampling in terms of percentage of the standard deviation σ_x.

According to our simulation the acquisition frequency should at least be 10, ideally 20 times larger than the corner frequency to avoid underestimating the standard deviation due to the effects of motion blur. Sampling just over the Nyquist frequency still underestimates the standard deviation by more than 30%. Based on our calculations we conclude that our video tracking data underestimate the position distribution by a factor of 2.5. Increasing the integration time of the acquired data even further by averaging over adjacent data points and plotting these experimental results shows good agreement with our simulated data in figure 4(a). This allows us to estimate the real corner frequency of our experiment to be approximately 300 Hz. We found that to monitor beam aberration correction a comparative analysis is sufficient. As σ is underestimated by the same factor for constant acquisition frequency, we are able to conclude that astigmatism correction improves the standard deviation of our trap by a factor of 3. We show the change in position distribution for different astigmatism settings in figure 5.

Video tracking of metal nanoparticles thus provides valuable information about the quality of an optical trap. It has been shown for micron-sized beads that the application of appropriate calibration and correction procedures allows precise corner frequency and power spectra to be recovered from undersampled and motion blur affected data [20, 21]. The application of these techniques should enable video tracking of nanoparticles in future experiments.

5. Conclusions

We presented a holographic tweezers workstation to manipulate and characterize metal nanoparticles. By combining techniques for trapping, beamshaping, imaging, particle tracking and spectroscopy we designed a tool to explore metal nanoparticles trapped in solution. We examined in detail the limiting factors of video tracking and came to the conclusion that it is possible to use video tracking for metal nanoparticles in certain circumstances, especially if there is no need for absolute accuracy. Single particle spectroscopy provides a tool to monitor particle–particle interactions; however, one needs to bear in mind that electrostatic forces may dominate over optical forces. The workstation provides the scope to be extended to measure trap stiffness and acquire more detailed information about the trapped nanoparticles and their interaction with light and their surroundings.

References

[1] Prikulis J, Svedberg F, Käll M, Enger J, Ramser K, Goksör M and Hanstorp D 2004 *Nano Lett.* **4** 115–8
[2] Tong L, Righini M, Gonzalez M U, Quidant R and Käll M 2009 *Lab Chip* **9** 193–5
[3] Guffey M J and Scherer N F 2010 *Nano Lett.* **10** 4302–8
[4] McDougall C, Stevenson D J, Brown C T A, Gunn-Moore F and Dholakia K 2009 *J. Biophoton.* **2** 736–43
[5] Kyrsting A, Bendix P M, Stamou D G and Oddershede L B 2011 *Nano Lett.* **11** 888–92
[6] Knight M W, Wu Y, Lassiter B, Nordlander P and Halas N J 2009 *Nano Lett.* **9** 2188–92
[7] Hansen P M, Bhatia V K, Harrit N and Oddershede L 2005 *Nano Lett.* **5** 1937–42
[8] Bosanac L, Aabo T, Bendix P M and Oddershede L B 2008 *Nano Lett.* **8** 1486–91
[9] Dienerowitz M, Mazilu M, Reece P J, Krauss T F and Dholakia K 2008 *Opt. Express* **16** 4991–9
[10] Jiang Y, Narushima T and Okamoto H 2010 *Nature Phys.* **6** 1005–9
[11] Padgett M J and Di Leonardo R 2011 *Lab Chip* **11** 1196–205

[12] Gibson G, Leach J, Keen S, Wright A and Padgett M J 2008 *Opt. Express* **16** 14561–70

[13] Berg-Sørensen K and Flyvbjerg H 2004 *Rev. Sci. Instrum.* **75** 594–612

[14] Ruh D, Tränkle B and Rohrbach A 2011 *Opt. Express* **19** 21627–42

[15] Keen S, Leach J, Gibson G and Padgett M J 2007 *J. Opt. A: Pure Appl. Opt.* **9** 264–26

[16] Otto O, Czerwinski F, Gornall J L, Stober G, Oddershede L B, Seidel R and Keyser U F 2010 *Opt. Express* **18** 22722–33

[17] Dienerowitz M, Gibson G, Bowman R and Padgett M 2011 *Proc. SPIE* **8097** 80971R

[18] Zijlstra P and Orrit M 2011 *Rep. Prog. Phys.* **74** 106401

[19] Pearce K, Wang F and Reece P J 2011 *Opt. Express* **19** 25559–69

[20] Wong W P and Halvorsen K 2006 *Opt. Express* **14** 12517–31

[21] van der Horst A and Forde N R 2010 *Opt. Express* **18** 7670–7

[22] www.physics.gla.ac.uk/Optics/projects/tweezers/software/

[23] Tong L, Miljković V D, Johansson P and Käll M 2011 *Nano Lett.* **11** 4505–8

[24] Ng J, Tang R and Chan C T 2008 *Phys. Rev.* B **77** 195407

[25] Wulff K, Cole D, Clark R, Di Leonardo R, Leach J, Cooper J, Gibson G and Padgett M J 2006 *Opt. Express* **14** 4170–5

[26] Dienerowitz M, Gibson G, Bowman R and Padgett M J 2011 *Opt. Express* **19** 24589–95